Forward-backward analysis of the photon-number evolution in a cavity

T. Rybarczyk,[1] B. Peaudecerf,[1] M. Penasa,[1] S. Gerlich,[1] B. Julsgaard,[2] K. Mølmer,[2] S. Gleyzes,[1] M. Brune,[1] J. M. Raimond,[1] S. Haroche,[1] and I. Dotsenko[1,*]

[1]*Laboratoire Kastler Brossel, Collège de France, CNRS, ENS-PSL Research University, UPMC-Sorbonne Universités, 11 place Marcelin Berthelot, 75005 Paris, France*

[2]*Department of Physics and Astronomy, Aarhus University, Ny Munkegade 120, DK-8000 Aarhus C, Denmark*

(Received 28 July 2014; revised manuscript received 27 January 2015; published 15 June 2015)

A quantum system can be monitored through repeated interactions with meter systems. The state of the system at time t, represented by the density matrix $\rho(t)$, then becomes conditioned on the information obtained by the meters until that time. More insight in the state of the system at any time t is provided, however, by taking into account the full detection of all meters interacting with the system both in the past and in the future of t. We present experiments that use near-resonant atomic probes to monitor the evolution of the quantized field in a cavity. The application of the forward-backward smoothing method to this quantum problem, justified by the past quantum state formalism [S. Gammelmark *et al.*, Phys. Rev. Lett. **111**, 160401 (2013)], allows us to resolve *a posteriori* dynamics, which is not reflected by the usual quantum state $\rho(t)$.

DOI: 10.1103/PhysRevA.91.062116 PACS number(s): 03.65.Ta, 03.65.Wj, 42.50.Pq

I. INTRODUCTION

Journalists' comments on the present time t are based on their knowledge of the present and of the past. It is sometimes difficult for them to single out the relevant events from the random noise of daily news or to lift ambiguities between equally probable interpretations. The situation of historians, working at a future time T, is quite different. They base their insights on all events up to their own time, and their knowledge of the future of t may be instrumental in sorting out the relevant events and in lifting ambiguities.

Similar considerations apply to the monitoring of the evolution of a classical or quantum system. In the classical realm, smoothing methods postprocess experimental data and compute the probabilities for the system to occupy different states at time t from the observations made both before and after t [1]. In particular, the forward-backward algorithm combines the conventional conditional probabilities, obtained by (forward) iteration of Bayes' rule until time t, with a (backward) iteration depending on all data obtained until the last observation at time T [1,2]. Direct application of these techniques to quantum systems has been realized for classical parameter estimation [3–6] and for the evolution of two-level systems [7–9]. A general quantum version of the forward-backward mechanism is provided by the past quantum state formalism [10]. It provides the best estimate about the result of any measurement performed on the system at t from information gathered in the past and in the future of t. Both in the classical case and in the quantum case, the estimation of properties at time t relies most strongly on measurement results obtained within a finite-time window before and after t. Contributions from much earlier and later detection events are suppressed due to the relaxation of the observed systems, described by rate processes.

In this paper, we apply the forward-backward method (or, equivalently, the past quantum state formalism) to the monitoring of the photon number in a microwave superconducting cavity mode, repeatedly probed by circular Rydberg atoms in the dispersive regime [11]. The atoms experience a photon-number-dependent light shift, which is read out using a Ramsey atomic interferometer. The probabilities of different atomic meter readings are periodic functions of the photon number n. By accumulating measurement results from meter atoms, we estimate the probability distribution for n at the end of the measurement and its time evolution in the past. This assignment is sensitive to statistical noise in the atomic detections, and ambiguities arise due to the periodicity of the detected signal versus n. The forward-backward estimation removes these ambiguities. It considerably reduces the statistical noise and reveals information about the system dynamics, which is hidden in the conventional, forward photon-number estimation. These results demonstrate the applicability and the benefits of this method in the quantum realm.

II. EXPERIMENTAL SETUP

The scheme of the setup is presented in Fig. 1. The microwave field is stored in a high-Q superconducting cavity C resonant at $\omega_c/2\pi = 51$ GHz [12]. The cavity, cooled down to 0.8 K, has an energy damping time $T_c = 65$ ms. It is repeatedly probed by circular Rydberg atoms, excited in B from a beam of Rubidium atoms propagating with a 250 m/s velocity. The atomic transition frequency ω_a between the circular states with principal quantum numbers 50 (state $|g\rangle$) and 51 (state $|e\rangle$) is close to ω_c. Atomic samples cross the cavity mode every $T_a = 86\,\mu$s. The atomic state is finally measured in the field-ionization detector D. On average, we detect 0.28 atom per sample.

The dispersive interaction of an atom with n photons in C changes the relative phase between $|g\rangle$ and $|e\rangle$ by $\varphi(n) \approx \varphi_0(n + 1/2)$, where φ_0 is the phase shift per photon [11]. Information on $\varphi(n)$, and thus on n, is read out using a Ramsey interferometer, made up of two low-Q cavities, R_1 and R_2, sandwiching C. They induce $\pi/2$ classical Rabi pulses between $|g\rangle$ and $|e\rangle$. Given a definite photon number n in the cavity, the conditional probability to detect the atom in state

*igor.dotsenko@lkb.ens.fr

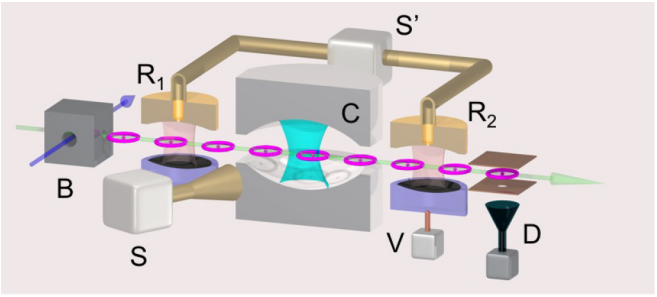

FIG. 1. (Color online) Scheme of the experimental setup. A sequence of circular Rydberg atoms crosses the mode of the high-finesse optical cavity C fed by microwave source S. The atomic states are excited in box B and detected in detector D. Auxiliary low-finesse cavities R_1 and R_2, fed by source S', constitute the Ramsey interferometer. The electric field produced in R_2 by the voltage V controls the interferometer phase.

$a \in \{g,e\}$ (the "Ramsey fringe signal") is

$$P(a|\phi,n) = \{1 \pm A \pm B(n)\,\sin[\varphi(n) - \varphi_0/2 - \phi]\}/2, \quad (1)$$

where the plus (minus) sign applies for $a = g$ (e) and ϕ is the Ramsey interferometer phase. Experimental imperfections account for the finite offset ($A = 0.03$) and the photon-number*dependent contrast $B(n)$. The contrast is $B(0) = 0.71$ for $n = 0$ and decreases with increasing n due to the spatial spread of the atomic beam in the cavity standing-wave mode (see Appendix A for details).

We set here the average phase shift per photon to $\varphi_0 \approx \pi/4$ by adjusting the atom-cavity detuning. In order to optimize the photon-number discrimination, the interferometer phase ϕ cycles through four values for successive atomic samples ($\phi_1 \approx 0$, $\phi_2 \approx \pi/4$, $\phi_3 \approx \pi/2$, and $\phi_4 \approx 3\pi/4$). It is controlled using a transient Stark shift of ω_a produced by the electric potential V applied across R_2. Due to the periodicity of $P(a|\phi,n)$, the measurement is *a priori* unable to distinguish n photons from $n + 8$ [13].

III. FORWARD-BACKWARD PHOTON-NUMBER ESTIMATION

Assume an initial photon-number probability distribution $P^f(n,0)$. This can be recursively updated by forward application of Bayes' rule [13],

$$P^f(n,t_i^+) \propto P(a_i|\phi_{r_i},n)P^f(n,t_i^-), \quad (2)$$

which relates the photon-number probabilities before (t_i^-) and after (t_i^+) detection of the ith atom in state a_i, probed with one of the phases ϕ_{r_i}, where $r_i = 1,\ldots,4$.

Similarly, in the time interval T_a between the atomic probe samples, the photon-number distribution $P^f(n,t)$ is subject to cavity relaxation described by the rate equation

$$\frac{dP^f(n,t)}{dt} = \sum_m K_{n,m}P^f(m,t), \quad (3)$$

where $K_{n,n} = -\kappa[(1+n_b)n + n_b(n+1)]$, $K_{n,n+1} = \kappa(1+n_b)(n+1)$, and $K_{n,n-1} = \kappa n_b n$, with all the other coefficients being zero [14,15]. In these expressions, $\kappa = 1/T_c$ is the field energy damping rate and $n_b = 0.074$ is the thermal photon number. Iterating Eqs. (2) and (3) until time t and normalizing the distribution to unity, we obtain the time-dependent photon-number distribution $P^f(n,t)$.

We now show that the forward-backward method [1,2] provides a better evaluation of the photon-number distribution at t based on information about the past as well as the future of t (detection events and relaxation). Such a method has recently been developed for monitored, dissipative quantum systems [10]. As we argue in Appendix B, the expressions for the diagonal elements of matrices applied in the full quantum treatment are, indeed, equivalent to the forward-backward formalism and hereby justify its application to the photon-number distribution in the cavity.

The forward-backward photon-number distribution reads

$$P^{fb}(n,t) = \frac{P^f(n,t)P^b(n,t)}{\sum_m P^f(m,t)P^b(m,t)}, \quad (4)$$

where the populations $P^f(n,t)$ are weighted by $P^b(n,t)$, the probability for the sequence of atomic meter readouts from t until T, conditioned on the photon-number measurement result n at time t. Following [1,2] (see also [7]), $P^b(n,t)$ depends on the measurement record $\{a_j\}$ ($t_j > t$) through the (backward) update equation,

$$P^b(n,t_j^-) \propto P(a_j|\phi_{r_j},n)P^b(n,t_j^+), \quad (5)$$

and between measurements, $P^b(n,t)$ solves the (backward) rate equation,

$$\frac{dP^b(n,t)}{d(-t)} = \sum_m K_{m,n}P^b(m,j), \quad (6)$$

where the values of $K_{m,n}$ are given after Eq. (3) (note the exchange of n and m). We shall normalize $P^b(n,t)$ separately and refer to it as the backward distribution.

The smoothing performed by the forward-backward method is conspicuous when we realize that the assignment of probabilities at two consecutive times t and $t + T_a$ differs only by the transfer of the last relaxation rate and Bayesian updates of $P^b(n,t+T_a)$ to the corresponding updates of $P^f(n,t)$.

While the past quantum state theory justifies the classical forward-backward method for the photon-number estimation, it is important to emphasize a conceptual difference between the interpretation of the results in the quantum and classical cases. Even when the quantum-mechanical density matrix $\rho(t)$ and the effect matrix of the past quantum state formalism $E(t)$ (see Ref. [10] and Appendix B for its definition) have only diagonal elements, corresponding to $P^f(n,t)$ and $P^b(n,t)$, we must distinguish the classical probability that the photon number *is* n from the quantum probability that the result of a photon-number *measurement* yields n.

The classical hidden Markov model formally deals with a hidden (classical) variable and thus associates $P^{fb}(n,t)$ with the probability that the system really occupies the number state $|n\rangle$. A hypothetical field quadrature measurement would then be governed by the probability $p(q,t) = \sum_n P^{fb}(n,t)|u_n(q)|^2$, where $u_n(q) = \langle q|n\rangle$ are harmonic oscillator eigenfunctions. But, according to Eq. (B2) in Appendix B, the past quantum state formalism yields a different expression: $p(q,t) = \mathcal{N}\sum_{nm} P^f(n,t)P^b(m,t)|u_n(q)|^2|u_m(q)|^2$, where $\mathcal{N}$ is a normalizing factor. We can apply the formalism of classical

smoothing, but even in experiments that are sensitive to only the photon number, this observable should not be thought of as a classical hidden variable, i.e., as a quantity with a stochastically evolving definite value.

IV. EXPERIMENTAL RESULTS

In a first experiment illustrating the achievements of the forward-backward state analysis, we inject photons in the cavity and then send a sequence of $S = 6500$ meter samples (total duration $T = 559$ ms). For the sake of experimental convenience we prepare initially a 6.2-photon coherent state. However, this information is discarded in our analysis in order to compare different photon-number estimation approaches independent of any *a priori* information on the field preparation. We thus set $P^f(n,0) = 1/16$ for $n = 0, \cdots, 15$.

Figure 2 shows a single realization of the experiment. We plot the forward, backward, and smoothed photon-number distributions versus time. The "noise" observed in P^f and P^b is mainly due to the statistical fluctuations of the random atomic detections [represented by the Bayesian updates (2) and (5), which can cause considerable changes in the photon-number distribution]. Between actual meter detections (occurring every 0.3 ms on average), $P^f(n,t)$ and $P^b(n,t)$ evolve continuously under cavity relaxation represented by the rate equations (3) and (6).

During the first 20 ms, the forward distribution in Fig. 2(a) exhibits two significant maxima, at $n = 0$ and $n \approx 8$, separated by the eight-photon period of the meter interferometric readout set by the choice $\varphi_0 \simeq \pi/4$. At $t \simeq 20$ ms, the most probable value of n jumps from 0 to 7, before relaxing toward zero in a series of downward jumps. In experiments where this large upward jump occurs, we are led to conclude that the outcome of a photon measurement before the jump was probably more likely to yield 8 than 0, a distinction we were, however, unable to make at that time.

The backward distribution $P^b(n,t)$ in Figs. 2(c) and 2(d) reflects the periodicity of $P(a|\phi,n)$ only at the end of the experimental sequence. Starting from time T, it quickly converges toward a mixture of n's close to 0 modulo 8. Then, at earlier times, down to $t \simeq 200$ ms, the combination of time-reversed decoherence and meter readings makes zero the most probable photon number. Continuing backward in time, the photon-number expectation value increases without any sign of the abrupt jumps by ± 8, which we saw for $P^f(n,t)$.

Figures 2(e) and 2(f) show the forward-backward distribution $P^{fb}(n,t)$, i.e., the normalized product of $P^b(n,t)$ and $P^f(n,t)$. The first striking observation is the drastic reduction of the noise [compare Fig. 2(f) to Figs. 2(b) and 2(d)]. In contrast to $P^f(n,t)$ and $P^b(n,t)$, $P^{fb}(n,t)$ includes the full available set of measurement and relaxation operators, and the almost equivalent significance of atoms measured before and after t implies a better signal-to-noise ratio in the state estimation. Also, some spiked changes in the number distribution $P^f(n,t)$ are discarded by the smoothing, as they are recognized as natural fluctuations in the detection events.

The highest outcome probability $\max_n\{P^{fb}(n,t)\}$ is, most of the time, larger than the corresponding $\max_n\{P^f(n,t)\}$. The outcome of a photon-number measurement and the times at which quantum jumps occur in the photon-number distribution are thus predicted with a higher fidelity by the forward-backward state analysis.

Finally, Figs. 2(e) and 2(f) clearly show that the ambiguity in the initial number distribution has been lifted, revealing information that is hidden in the standard forward analysis in Figs. 2(a) and 2(b). We can identify the series of quantum jumps from the initial n, around 9 in this example, down to vacuum. These features illustrates how detection results obtained after time t can radically change state estimation at t.

We assess the quality of the conventional and the smoothed state predictions by comparing, in a single realization of the experiment, the photon-number distributions obtained from two disjoint subsets of atomic data. These distributions are both nonexhaustive estimates of the same measurement outcome distribution, and their mutual discrepancies reflect how much their predictions vary from a real measurement.

We obtain the photon-number distribution by repeating the experiment of Fig. 2 $N_r = 6000$ times. For each realization $k = 1, \ldots, N_r$, we sort the atomic samples into two independent subsets, A_k and B_k. The first four samples go into A_k, the next four into B_k, etc. The four Ramsey phases are thus equally represented in A_k and B_k. Using the data of each subset separately, we compute the forward and smoothed distributions, $P^f_{u_k}(n,t)$ and $P^{fb}_{u_k}(n,t)$, where $u_k = \{A_k, B_k\}$, and their average photon numbers $\bar{n}^m_{u_k}(t)$, where $m \in \{f, fb\}$. We finally quantify the distance between the distributions provided by the A and B data subsets using the root-mean-square deviation (over a large number of experimental runs) of the time-dependent estimate of the mean photon numbers $\Delta^m(t)$:

$$\Delta^m(t) = \sqrt{\frac{\sum_{i=1}^{N_r} \left(\bar{n}^m_{A,i}(t) - \bar{n}^m_{B,i}(t)\right)^2}{N_r}}. \tag{7}$$

Figure 3 shows the result of this comparison for the forward and forward-backward analyses (solid thin green and thick red lines, respectively). The deviation $\Delta^{fb}(t)$ is, for nearly all times, much smaller than $\Delta^f(t)$, indicating that the smoothed state analysis provides a better estimate of the photon-number distribution. Note, however, that, for $t < 14$ ms, $\Delta^f(t) < \Delta^{fb}(t)$ since the forward distributions are identical at $t = 0$, and even though they are very broad and imprecise, $\Delta^f(0) = 0$. The statistically independent information provided by disjoint sets of atomic samples, however, quickly results in a rapid increase of $\Delta^f(t)$, followed by a slow decrease due to the narrowing of the photon-number distributions induced by cavity relaxation and by the information retrieved by the measurements.

We now present a second experiment applying the forward-backward analysis to the detection of a photon-number quantum jump induced on purpose at a well-defined time. The experimental sequence involves three parts. Starting with the residual thermal field, which is close to vacuum, we first transmit 4000 meter samples. We then induce a photon creation quantum jump by injecting a single sample prepared in $|e\rangle$. Using the Stark effect produced by an electric-field pulse applied across the cavity mirrors, we tune this sample in resonance with C, leading to atomic emission with a high probability. We then resume the measurement of the field with 4000 nonresonant meter samples. The experiment is repeated

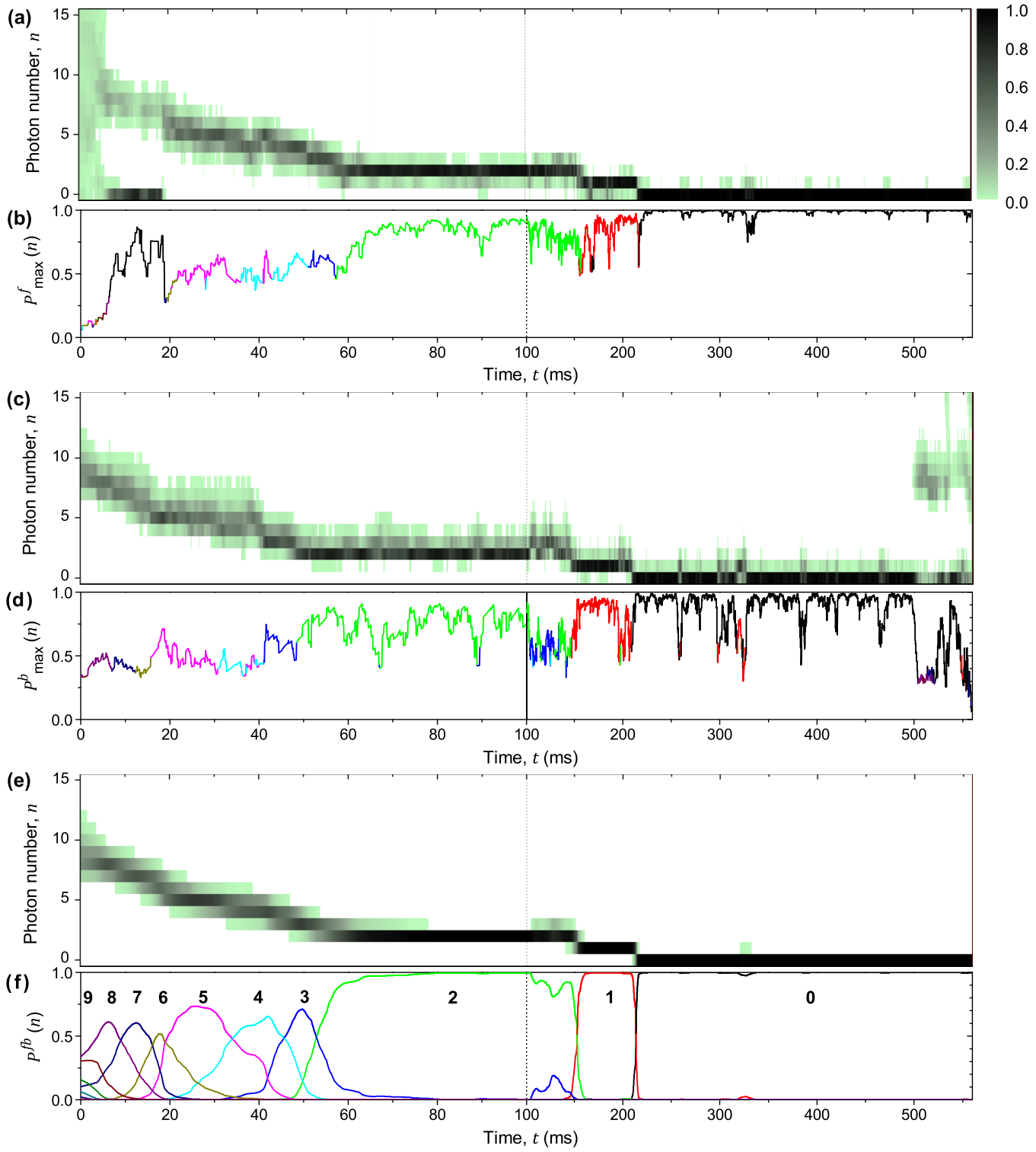

FIG. 2. (Color online) Evolution of the estimated photon-number distributions. (a) and (b) Forward, (c) and (d) backward, and (e) and (f) smoothed distributions in a typical realization of the experiment. (a), (c), and (e) present probabilities with the color shade scale given in (a). (b), (d), and (f) give the explicit evolution of the photon-number probabilities. For the sake of clarity, we plot only the probability of the most likely photon number in (b) and (d). This number is given by the line color code, defined by the labels in (f). Note that the time scale on the horizontal axis is changed by a factor of about 5 at $t = 100$ ms (vertical dotted line) for all panels.

16 320 times. We select the 2962 realizations with exactly one atom detected in state $|g\rangle$ in the resonant sample. We thus isolate the sequences in which a quantum jump has most likely been successfully induced.

Figure 4 shows the mean photon number obtained from the forward (solid thin green line), backward (dashed blue line), and forward-backward (solid thick red line) analyses. Figure 4(a) presents a single realization. The time origin,

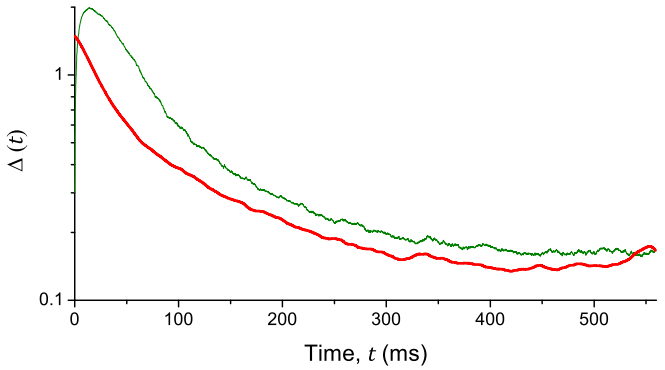

FIG. 3. (Color online) Root-mean-square deviations, $\Delta^{fb}(t)$ (thick red line) and $\Delta^{f}(t)$ (thin green line), between mean photon numbers reconstructed from two independent subsets of data measured on the same experimental realizations.

$t = 0$, corresponds to the induced jump. As expected, the forward (backward) measurement detects the induced jump later (earlier) than its real occurrence time. The smoothed state analysis gives a much better estimate: the jump time, defined as the time when the expected mean value of the photon-number measurement crosses the 0.5 level, is much closer to zero. The standard deviation of all jump times is 4.4 ms, corresponding to 13 detected atoms.

Figure 4(b) shows an average over all selected realizations. The forward-backward curve crosses the 0.5 level at 0.1 ms, a deviation from zero shorter than the delay between two detected atoms. This demonstrates that the smoothed estimation of the jump time is unbiased. In comparison, the average jump detection with standard analysis is delayed by about 10 ms.

The black line is an exponential fit of the forward-backward state data obtained for $t > 35$ ms. The fit parameters are the decay constant, 67 ms (close to the independently determined T_c), an offset of 0.068 photon (close to n_b), and an amplitude of 1.27 at $t = 0$. This initial photon number is higher than 1 and can be explained by the events in which two atoms in the resonant sample (one remaining undetected) inject two photons into C. This value is in excellent agreement with a prediction based on the efficiency of D (30%) and the Poisson distribution of the atom number in each sample.

The study of quantum jumps can be extended to larger photon numbers. We have applied the forward-backward analysis to the data of the 6000 experiments used for Fig. 3 with an initial coherent state having $P^{f}(n,0) = e^{-\bar{n}_0}\bar{n}_0^n/n!$ with $\bar{n}_0 = 6.2$ photons. For each trajectory, we determine the time intervals during which different number states have the highest probability. Using data from all trajectories, we get, for each n, the distribution of these time intervals, and we find that it nicely fits with an exponential decay (see Appendix C for details). This fit provides the lifetimes $T_n^{\rm exp}$ of the Fock states with $1 \leqslant n \leqslant 10$ (higher Fock states lead to poor statistics and large uncertainties). They are plotted as red circles in Fig. 5.

The theoretical values of these lifetimes are $T_n^{\rm th} = T_c/[n(1+n_b)+n_b(n+1)]$. They are shown as black squares in Fig. 5 and are in excellent agreement with the values extracted from the evolution of $P^{fb}(n,t)$. These theoretical values had already been confirmed experimentally in [15] by analyzing the evolution of photon-number distributions averaged over many experimental realizations. Here, in contrast, we extract the information from the analysis of individual quantum jumps, an impossible feat using the forward analysis.

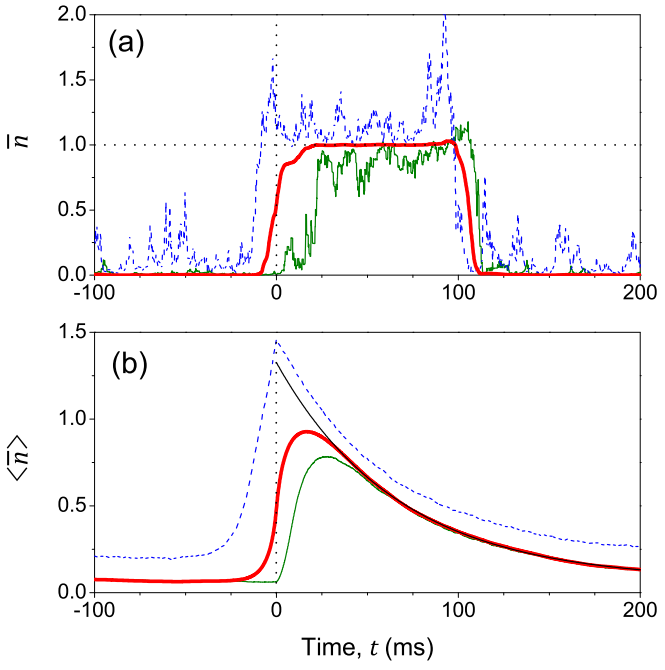

FIG. 4. (Color online) Detection of a photon creation quantum jump induced at $t = 0$. (a) Evolution of the mean photon number $\bar{n}$ in the forward (solid thin green line), backward (dashed blue line), and forward-backward (solid thick red line) analyses for a single realization. (b) Average over 2962 realizations $\langle\bar{n}\rangle$. The black line is an exponential fit to the smoothed result.

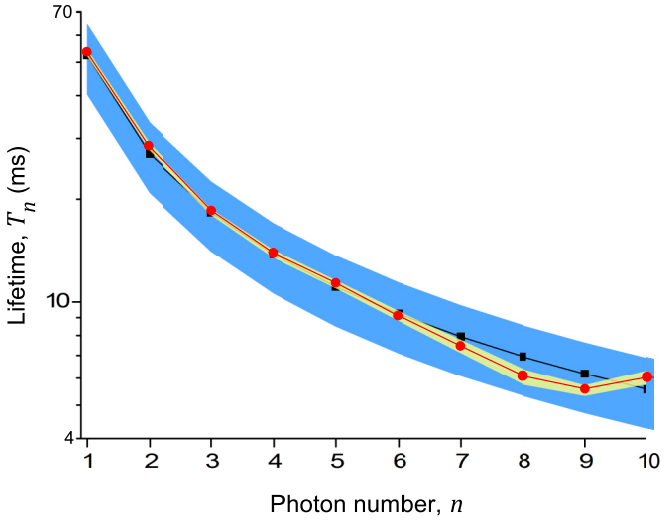

FIG. 5. (Color online) Lifetimes of the photon-number states. The red circles present the experimental results; the light yellow (light gray) band presents the bounds of the experimental values of $T_n^{\rm exp}$ reconstructed with the *a priori* value of T_c varying from 50 to 80 ms. The black squares are the theoretical values $T_n^{\rm th}$; the dark blue (dark gray) band presents their bounds for 50 ms $< T_c <$ 80 ms.

Moreover, we determine the lifetimes of Fock states with $n > 7$, which cannot be detected unambiguously in the forward analysis.

The forward-backward state analysis uses an *a priori* knowledge of the cavity lifetime, $T_c = 65$ ms [see Eqs. (3) and (6)]. In order to check that the inferred values of $T_n^{\rm exp}$ are not merely reproducing this knowledge, we have performed the analysis with different choices of T_c between 50 and 80 ms. The corresponding theoretical values $T_n^{\rm th}$ are given by the wide blue (dark gray) band in Fig. 5. The measured $T_n^{\rm exp}$ values are presented as the narrow yellow (light gray) band around the red circles. The small variation of $T_n^{\rm exp}$'s for a large span of T_c clearly shows that the measured values are not appreciably biased by the damping model introduced in the smoothed state reconstruction.

V. SUMMARY

We have applied the forward-backward analysis of classical hidden Markov models to the state of a quantum field in a cavity. This postprocess analysis is validated by the full quantum theory of measurements, and it applies here because coherences between photon-number states are not measured and do not influence the population dynamics. By using meter atom readouts, before and after time t, we get a better estimate of the photon-number dynamics than with the standard approach, which uses only information available at and before t. By removing ambiguities in the photon-number evolution, we access information which is hidden in the standard approach, and we observe an improved temporal correlation between our state assignment and the deterministic injection of a photon into the cavity. Finally, from a more precise determination of the quantum jump times, we extract photon-number state lifetimes and verify that they very precisely follow exponential distributions. All these features confirm the validity of the forward-backward method in this quantum context, and they show its power for the analysis of the dynamics of quantum systems.

ACKNOWLEDGMENTS

The authors acknowledge support from the European Research Council (DECLIC project), the European Community (SIQS project), and Agence Nationale de la Recherche (QUSCO-INCA project). M.P. acknowledges support from Direction Générale de l'Armement (DGA) of the French Ministry of Defence. S.G. acknowledges support be the European Community FP7/2007-2013 Contract No. 626628 (Marie-Curie Actions). B.J. and K.M. acknowledge support from the Villum Foundation.

APPENDIX A: CALIBRATION OF THE MEASUREMENT OPERATORS

A reliable state reconstruction requires excellent knowledge of all measurement parameters. In our case, the conditional probabilities $P(a|\phi,n)$ must be calibrated as carefully as possible before analyzing the data. The relevant parameters [14] are the phase shifts $\varphi(n)$, the Ramsey interferometer phases ϕ_j $(j = 1,\ldots,4)$, the offset A, and the contrast $B(n)$. The particularly important parameters for extracting the most information on large photon numbers are $\varphi(n)$ and $B(n)$.

The calibration of the dephasing $\varphi(n)$ is presented in detail in Ref. [14]. In the large detuning regime and for small photon numbers, $\varphi(n)$ depends linearly on n. In our case, however, there is weak nonlinearity, which has to be carefully taken into account. For the current experimental parameters (atom-cavity detuning $\delta/2\pi = 248$ kHz and vacuum Rabi frequency $\Omega_0/2\pi = 46$ kHz) we have found $\varphi(n) = 0.250\pi(n + 1/2) - 0.0011\pi n^2$.

Due to the spatial spread of the atomic beam along the cavity axis (about 0.7 mm), all atoms do not experience the same coupling Ω_0 to the cavity mode. This spread induces a dispersion of the phase shifts $\varphi(n)$. The average Ramsey fringe contrast is thus a decreasing function of n. Since the exact position and spread of the atomic beam cannot be measured directly, we use a method based on atomic spin tomography to reconstruct $B(n)$.

In Refs. [14,15] we have used the distribution of the transverse atomic pseudospin after interaction with the cavity field to determine $\varphi(n)$. Here, we use the same method to extract also information on the contrast $B(n)$, which amounts to a reduction of the spin amplitude with φ (and thus with n). We analyze the experimental data used for Fig. 3. For all experimental realizations and for every ensemble of 200 successive atomic samples, we calculate the relative atomic population in state g, R_j, detected with the Ramsey phase ϕ_j. It is defined as

$$R_j = \frac{m_{g,j} - m_{e,j}}{m_{g,j} + m_{e,j}} + A/2, \tag{A1}$$

where $m_{a,j}$ is the number of atoms in the jth ensemble detected in state $a \in \{g,e\}$ and $A = 0.03$ is the independently measured Ramsey fringe offset. Next, we calculate components σ_x and σ_y of the atomic pseudospin:

$$\sigma_x = \frac{1}{2}\left[\frac{R_3 - R_1\cos\phi_3}{\sin\phi_3} + \frac{R_2\cos\phi_4 - R_4\cos\phi_2}{\sin[\phi_2 - \phi_4]}\right],$$
$$\sigma_y = \frac{1}{2}\left[R_1 + \frac{R_2\sin\phi_4 - R_4\sin\phi_2}{\sin[\phi_4 - \phi_2]}\right]. \tag{A2}$$

All experimental realizations start with a coherent field of 6.2 photons on average. In order to avoid the overlap of different photon numbers due to the eight-photon periodicity of the interferometric measurement, we isolate three separate sets of data for which the probability to have a photon number in the ranges $n \in [0,7]$, $[4,11]$, and $[8,15]$ is higher than 0.8, respectively. This selection is performed using $P^{fb}(n,t)$ distributions calculated with a constant Ramsey fringe contrast B. This rough estimate is sufficient to isolate the proper ranges of photon numbers.

The spin tomography is then performed independently on these three sets. The corresponding results are shown as histograms in Figs. 6(a), 6(b), and 6(c). The white spiral lines in each panel are a guide to the eye to follow the reduction of the spin amplitude with n. This tomography does not provide a direct measurement of $B(n)$ since it is also affected by spontaneous quantum jumps occurring during the 200-sample time interval (i.e., during 17.2 ms) used to calculate σ_x and σ_y.

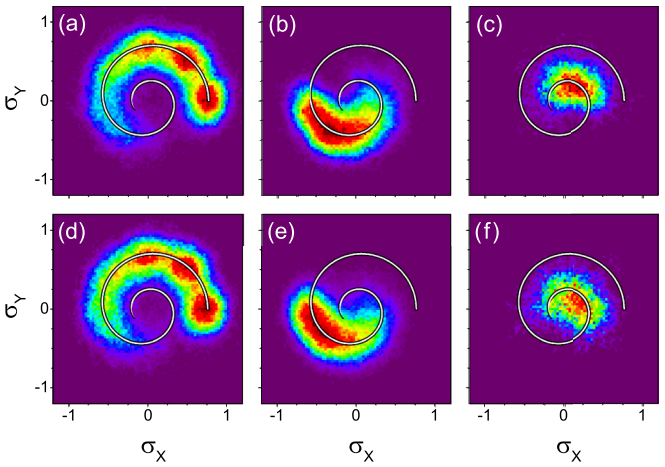

FIG. 6. (Color online) Spin tomography. (a), (b), and (c) Experimental data for three ranges of field values. (d), (e), and (f) Simulation results for the same ranges. The conditional probability $P(e|\phi,n)$, used in this simulation, is shown in Fig. 7. The white line (the same in all panels) is a guide to the eye.

In order to determine $B(n)$, we numerically simulate the experiment with various forms of $B(n)$ and search the one which best reproduces the experimental data. Figures 6(d), 6(e), and 6(f) present these simulation results. They are in excellent agreement with the experimental data. The corresponding optimal Ramsey fringes $P(e|\phi_j,n)$ are shown in Fig. 7. These conditional probabilities have been used to reconstruct all forward and smoothed photon-number distributions presented in this paper.

This approach is confirmed by a detailed analysis of the atom-cavity coupling dispersion due to the atomic beam spread. The optimal fringes $P(e|\phi_j,n)$ correspond to a circular atomic beam with a 0.8-mm diameter displaced vertically 0.39 mm away from the cavity center. These parameters are quite realistic for our experimental setup. They also explain the observed value of the Rabi frequency (46 kHz), which is smaller than the maximal coupling of 50 kHz computed at the cavity center.

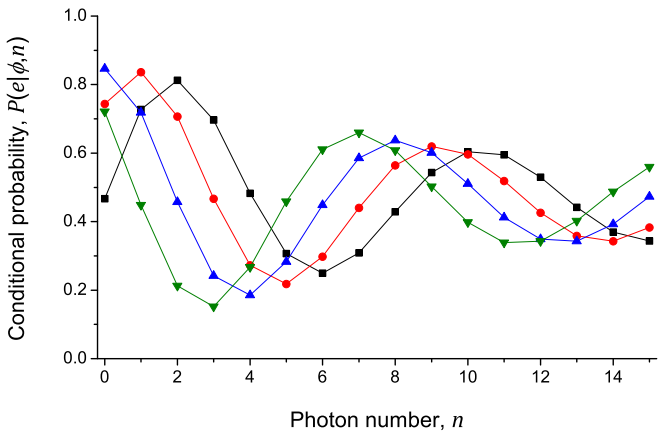

FIG. 7. (Color online) Conditional probability $P(e|\phi,n)$ to detect an atom in state e. The four curves correspond to the four Ramsey interferometer phases ϕ used in the experiment: $\phi_1 = 0$ (squares), $\phi_2 = 0.260\pi$ (circles), $\phi_3 = 0.519\pi$ (triangles), and $\phi_4 = 0.773\pi$ (diamonds). The contrast reduction is found by matching the simulation results of the atomic spin distribution with the experimental one (see Fig. 6).

APPENDIX B: THE PAST QUANTUM STATE FORMALISM

In quantum mechanics, the density matrix $\rho(t)$ accounts for the maximum information available about a quantum system at time t. Thus, $\rho(t)$ provides the probabilities for the outcome of any quantum measurement, generally described by positive operator-valued measures (POVMs) $\{\hat{\Omega}_n^\dagger\hat{\Omega}_n\}$ [16]:

$$p(n) = \mathrm{Tr}[\hat{\Omega}_n^\dagger\hat{\Omega}_n\rho(t)]. \tag{B1}$$

The value of $\rho(t)$ is found by solving equations that take into account the system Hamiltonian, coupling to ancillary quantum systems, and measurements, carried out either directly on the system or on the ancillary degrees of freedom. In many situations, damping and dissipation caused by the coupling to an environment may be taken into account by a Lindblad master equation, $d\rho/dt = \mathcal{L}[\rho]$, with terms of the form $\hat{C}_i\rho\hat{C}_i^\dagger - \frac{1}{2}(\hat{C}_i^\dagger\hat{C}_i\rho + \rho\hat{C}_i^\dagger\hat{C}_i)$. Lindblad terms $\hat{C}_1 = \sqrt{\kappa(n_b+1)}\hat{a}$ and $\hat{C}_2 = \sqrt{\kappa n_b}\hat{a}^\dagger$ with photon annihilation (creation) operators $\hat{a}$ ($\hat{a}^\dagger$) thus describe the exchange of photons between a cavity mode and a thermal heat bath and yield the rate equation for $P^f(n,t)$ (3) when restricted to the diagonal elements $\rho_{nn}(t)$ of the density matrix.

Probing a quantum system by an ancillary meter system is described by the evolution and subsequent reduction of the joint system and meter state, depending on the random outcome μ of the measurement on the ancilla. Discarding the meter after the measurement, this leaves the system in a new density matrix, $\rho \to \hat{L}_\mu\rho\hat{L}_\mu^\dagger$, with POVM operators $\{\hat{L}_\mu^\dagger,\hat{L}_\mu\}$. Measurements may be imperfect due to, for example, finite detector efficiency or unresolved ancilla properties. In our experiment, for example, atoms may pass undetected, we may mistake a ground for an excited atom, and we may detect only one atom when more atoms have actually passed the cavity [14]. This can be taken into account by associating with an outcome μ' a (coarse grained) weighted back action, $\rho \to \sum_\mu P(\mu'|\mu)\hat{L}_\mu\rho\hat{L}_\mu^\dagger$. When all these features and their consequences for the evolution of the diagonal elements of the density matrix are included for our cavity system, we recover the transformation (2), following from the Bayes' rule argument.

When we are only concerned with measurements of the photon number, i.e., $\hat{\Omega}_n = \hat{\Omega}_n^\dagger = |n\rangle\langle n|$, (B1) yields the usual result, $p(n) = \rho_{nn}(t)$. The probability to get n in a photon-number measurement is the population of the number state $|n\rangle$ according to the density matrix.

In a recent paper [10], it was shown that the probabilities that we can assign at time T to the outcome of general quantum measurements on a quantum system at an earlier time t are conditioned not only on the dynamics of the system until time t but also on the dynamics from t to T. Specifically, the probing of the system after t yields information about the earlier state. This theory does not change the density matrix $\rho(t)$, but it

assigns different probabilities for measurement outcomes than Eq. (B1).

To obtain the refined outcome probability for the measurement at time t, we must supplement the density matrix $\rho(t)$ with an "effect matrix" $E(t)$, which is obtained as a product of matrices, corresponding to a backward evolution in time by measurement back action and relaxation between T and t. The theory yields a factorization of the probability,

$$P^{fb}(n,t) = \frac{\mathrm{Tr}[\hat{\Omega}_n \rho(t) \hat{\Omega}_n^\dagger E(t)]}{\sum_m \mathrm{Tr}[\hat{\Omega}_m \rho(t) \hat{\Omega}_m^\dagger E(t)]}. \tag{B2}$$

Expression (B2) leads to considerable modification of the conventional predictions based on (B1). In the appropriate weak and strong measurement limits, Eq. (B2) reproduces both Aharonov's "weak values" [17,18] and the Aharonov-Bergmann-Lebowitz rule [19] for pre- and postselected measurements. Equation (B2) has been used for the interpretation of weak measurements on a qubit undergoing projective measurements at zero and T [20] and for continuous monitoring by homodyne detection of a superconducting qubit in a microwave cavity [21].

In our case, where the probing by atom meters is sensitive to only the photon numbers, the diagonal elements $E_{nn}(t)$ solve a closed set of equations, readily identified as Eqs. (5) and (6) for $P^b(n,t)$ in this article. The dynamics of E is adjoint to the dynamics of $\rho(t)$ [10], in agreement with the swap of indices on the rate coefficients between Eqs. (3) and (6). As long as we want to make only predictions for photon-number measurements, the classical smoothing theory, Eq. (4), relying on Bayes's rule and hidden Markov model dynamics, is therefore equivalent to the past quantum state expression (B2).

APPENDIX C: PHOTON-NUMBER LIFETIMES

We extract information on the photon-number lifetimes, presented in Fig. 5, from the data acquired in 6000 realizations of the experiment. Each experimental sequence starts by injecting into the cavity a coherent field with a mean photon number $\bar{n}_0 = 6.2$. The information on this initial field is used in the forward-backward analysis by setting $P^f(n,0) = e^{-\bar{n}_0} \bar{n}_0^n / n!$. The state reconstruction in each realization is performed with 6500 atomic samples. Note that the same data set has also been used for Fig. 3.

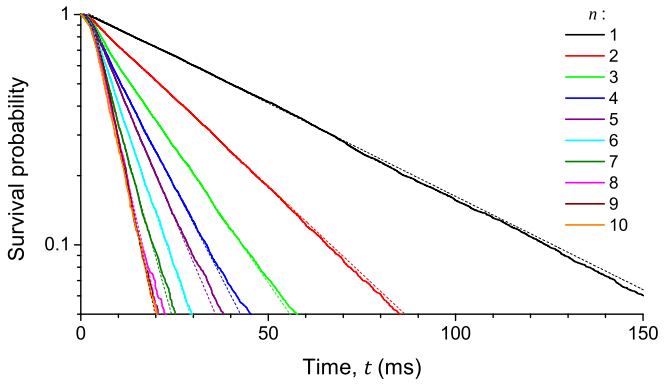

FIG. 8. (Color online) Survival probability of photon numbers n from 1 to 10 vs time. Thick solid lines are experimental data; thin dashed lines are exponential fits.

We define a quantum jump as the time when the most probable photon number n changes. For each n, we search all its appearances in all realizations and measure the corresponding time intervals of its survival. Next, we calculate the probability to survive versus time and, finally, fit an exponential decay function, $f(t) = A \exp(-t/T_n)$, to these data. Figure 8 shows experimental data and fit results as solid and dashed lines, respectively. Since we cannot reliably resolve very short times between successive jumps, all fits start at 8 ms (about 30 detected atoms). The fitted T_n values are shown in Fig. 5. Only photon numbers up to 10 have been analyzed here since for larger n's the measurement statistics is very poor.

[1] W. H. Press, S. A. Teukolsky, W. T. Vetterling, and B. P. Flannery, *Numerical Recipes: The Art of Scientific Computing*, 3rd ed. (Cambridge University Press, New York, 2007).

[2] R. Rabiner, A tutorial on hidden Markov models and selected applications in speech recognition, Proc. IEEE **77**, 257 (1989).

[3] M. Tsang, Time-symmetric quantum theory of smoothing, Phys. Rev. Lett. **102**, 250403 (2009).

[4] M. Tsang, Optimal waveform estimation for classical and quantum systems via time-symmetric smoothing, Phys. Rev. A **80**, 033840 (2009).

[5] M. Tsang, Optimal waveform estimation for classical and quantum systems via time-symmetric smoothing. II. Applications to atomic magnetometry and Hardy's paradox, Phys. Rev. A **81**, 013824 (2010).

[6] M. Tsang, H. M. Wiseman, and C. M. Caves, Fundamental quantum limit to waveform estimation, Phys. Rev. Lett. **106**, 090401 (2011).

[7] S. Gammelmark, K. Mølmer, W. Alt, T. Kampschulte, and D. Meschede, Hidden Markov model of atomic quantum jump dynamics in an optically probed cavity, Phys. Rev. A **89**, 043839 (2014).

[8] M. A. Armen, A. E. Miller, and H. Mabuchi, Spontaneous dressed-state polarization in the strong driving regime of cavity QED, Phys. Rev. Lett. **103**, 173601 (2009).

[9] J. Kerckhoff, M. A. Armen, D. S. Pavlichin, and H. Mabuchi, The dressed atom as binary phase modulator: Towards attojoule/edge optical phase-shift keying, Opt. Express **19**, 6478 (2011).

[10] S. Gammelmark, B. Julsgaard, and K. Mølmer, Past quantum states of a monitored system, Phys. Rev. Lett. **111**, 160401 (2013).

[11] S. Haroche and J. M. Raimond, *Exploring the Quantum: Atoms, Cavities, and Photons* (Oxford University Press, Oxford, 2006).

[12] S. Kuhr, S. Gleyzes, C. Guerlin, J. Bernu, U. B. Hoff, S. Deléglise, S. Osnaghi, M. Brune, J.-M. Raimond, S. Haroche, E. Jacques, P. Bosland, and B. Visentin, Ultrahigh finesse Fabry-Pérot superconducting resonator, Appl. Phys. Lett. **90**, 164101 (2007).

[13] C. Guerlin, J. Bernu, S. Deléglise, C. Sayrin, S. Gleyzes, S. Kuhr, M. Brune, J.-M. Raimond, and S. Haroche, Progressive field-state collapse and quantum non-demolition photon counting, Nature (London) **448**, 889 (2007).

[14] B. Peaudecerf, C. Sayrin, X. Zhou, T. Rybarczyk, S. Gleyzes, I. Dotsenko, J. M. Raimond, M. Brune, and S. Haroche, Quantum feedback experiments stabilizing Fock states of light in a cavity, Phys. Rev. A **87**, 042320 (2013).

[15] M. Brune, J. Bernu, C. Guerlin, S. Deléglise, C. Sayrin, S. Gleyzes, S. Kuhr, I. Dotsenko, J. M. Raimond, and S. Haroche, Process tomography of field damping and measurement of Fock state lifetimes by quantum nondemolition photon counting in a cavity, Phys. Rev. Lett. **101**, 240402 (2008).

[16] M. A. Nielsen and I. L. Chuang, *Quantum Computation and Quantum Information* (Cambridge University Press, Cambridge, 2000).

[17] Y. Aharonov and L. Vaidman, Complete description of a quantum system at a given time, J. Phys. A **24**, 2315 (1991).

[18] H. M. Wiseman, Weak values, quantum trajectories, and the cavity-QED experiment on wave-particle correlation, Phys. Rev. A **65**, 032111 (2002).

[19] Y. Aharonov, P. G. Bergmann, and J. L. Lebowitz, Time symmetry in the quantum process of measurement, Phys. Rev. **134**, B1410 (1964).

[20] P. Campagne-Ibarcq, L. Bretheau, E. Flurin, A. Auffèves, F. Mallet, and B. Huard, Observing interferences between past and future quantum states in resonance fluorescence, Phys. Rev. Lett. **112**, 180402 (2014).

[21] D. Tan, S. J. Weber, I. Siddiqi, K. Mølmer, and K. W. Murch, Prediction and retrodiction for a continuously monitored superconducting qubit, Phys. Rev. Lett. **114**, 090403 (2015).